Journal of Materials Chemistry A

Accepted Manuscript

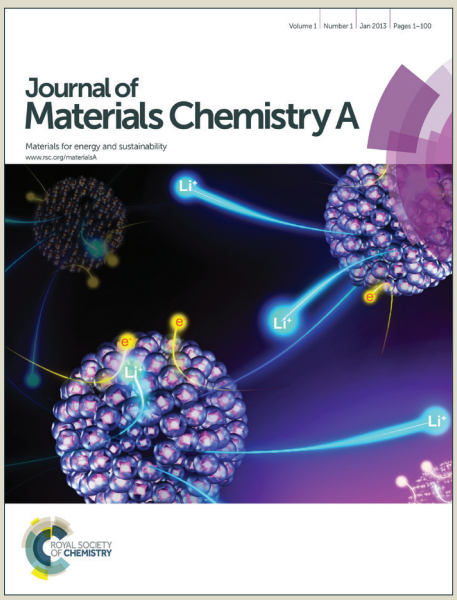

ROYAL SOCIETY OF CHEMISTRY

www.rsc.org/materialsA

Journal of Materials Chemistry A RSCPublishing

ARTICLE

Graphene/Silk Fibroin Based Carbon Nanocomposites for High Performance Supercapacitors

Cite this: DOI: 10.1039/x0xx00000x

Received 00th January 2012,
Accepted 00th January 2012

DOI: 10.1039/x0xx00000x

www.rsc.org/

Yaxian Wang, [a] Yanfang Song, [b] Yu Wang, [a] Xin Chen, [a] Yongyao Xia, [b] Zhengzhong Shao*[a]

The graphene and silk fibroin based carbon (GCN-S) material is prepared by carbonization of the reduced graphene oxide (RGO) and silk fibroin (SF) nanofibrils composite in the presence of KOH. The well combination of RGO and SF nanofibrils, which turns out to be micro/meso- carbon after activation, endows the obtained GCN-S materials with high specific surface area, multi-porous structure, good electrical conductivity, and the consequently excellent electrochemical performance. For example, the GCN-S-0.5 synthesized at 0.5:1 ratio of KOH and RGO/SF nanofibrils suspension shows high BET specific surface area of 3.2×10^3 m^2 g^{-1}, and the specific capacitance is 256 F g^{-1} at the current density of 0.5A g^{-1}. Moreover, it still delivers a specific capacitance of 188 F g^{-1} even at the current density as high as 50 A g^{-1}, corresponding to a capacitance retention rate of 73.4%. After charge–discharge rate of 5 A g^{-1} for 10000 cycles, the GCN-S-0.5 exhibits remarkable electrochemical stability with the capacitance retention ratio of 96.3%. Furthermore, the GCN-S-0.5 based supercapacitor achieves high energy density up to 14.4 Wh kg^{-1} at an ultrahigh power density of 40000 W kg^{-1}. The results shown in this work imply that our GCN-S material is a promising candidate for manufacturing the supercapacitors with both high performance and relatively low cost.

Introduction

Supercapacitors, as a promising candidate for power sources and energy-storage devices, have triggered intensely attention due to their high-impact characteristics, such as high power capability, fast energy delivery, superior reversibility, long cycle life, wide thermal operating range, and low maintenance cost.[1-3] Based on their energy storage mechanism, supercapacitors can be divided into two categories,[4] which is electrochemical double-layer capacitors (EDLCs) and pseudo-capacitors. Among them, EDLCs, the most common devices at present, use carbon-based active materials with high surface area, including activated carbon (AC), mesoporous carbon, carbon nanotubes, and carbide-derived carbon.[5] However, the limited energy storage capacity and rate capability restrict their applications only to certain niche markets.[6] On the other hands, pseudo-capacitors have been actively pursued as they can achieve higher capacitance than EDLCs, due to the redox process of electroactive materials.[7, 8] However, the poor electrical conductivity, the easy structure damage during the redox process as well as the lack of a pure cycling stability bring a huge resistance for their practical applications.[9]

Recently, there is a huge enthusiasm in obtaining carbon-based materials derived from natural polymers, such as silk proteins,[10] human hair,[11] egg-white[12] or other biomass sources including dead leaves,[13] cellulose,[14] potato starch,[14] eucalyptus wood sawdust,[14] pollens,[15] and cow dung[16]. By doping of heteroatoms and creating proper pore size distribution, such materials combine the advantage of EDLCs and pseudo-capacitors materials to exhibit high specific capacitance at a low current density, but most of them still suffer the huge capacity damage problem at the high current density.

Graphene is regarded as one of the most suitable substrate materials for preparing pseudo-capacitor electrodes,[17, 18] due to its large surface area, excellent structural stability, as well as superb electrical and thermal conductivities.[19-24] The graphene-based pseudo-capacitor composite materials of various structures, such as MnO_2–graphene foam, sandwich structure of graphene nanosheets and oxide nanoparticle, flexible graphene-polyaniline composite paper, have been prepared via multifarious ways.[25-30] With the existence of graphene, the electrical performance of these pseudo-capacitor composite materials has been improved to a certain extent. However, the most approaches to obtain these materials were either complicated or hard to realize the uniform dispersion of graphene and electroactive materials at nanoscale, which largely weakened the advantages of graphene.

A number of biomolecules, such as nucleotides,[31] peptides,[32] and proteins[33] are found to be able to interact with graphene oxide (GO) or reduced graphene oxide (RGO) by electrostatic and interactions to form different hybrid structures.[34] Thus, people developed corresponding biomolecules-graphene based materials for various applications, such as peptide enabled graphene biosensor for selective detection of target proteins,[35] graphene-nanoparticle hybrid sensor for enzyme detection,[36] biodegradable nanocomposites of amyloid fibrils and graphene with shape-memory and enzyme-sensing properties,[37] chitosan/GO based aptasensor for the

impedimetric detection of lysozyme,[38] and so on. Silk Fibroin (SF), a natural fibrous protein with amphiphilic properties derived from silkworm silk, is another great candidate. By adjusting the hydrogen bonding and hydrophobic interactions, a few of SF-based hybrid materials such as SF-carbon nanotube film[39], SF-GO film[40, 41] and SF-RGO film[42] are prepared as high-strength structural materials and so on.

In this work, we obtained a well-combined RGO/SF based carbon nanocomposite (GCN-S) through a novel and efficient way. Firstly, we prepared a rather stable and homogeneous suspension of RGO sheets fully covered with SF nanofibrils by the directly assembling of SF macromolecules on the RCO surface. Afterwards, by adding a small amount of alkali for activation, we harvest the GCN-S after carbonizing the freeze-dried RGO/SF nanofibrils aerogels. The resulting GCN-S material was then applied as an electrode material for supercapacitor in 6 mol/L KOH aqueous using a three-electrode system with an Hg/HgO reference electrode and a platinum counter electrode at room temperature. Prospectively, the GCN-S exhibits excellent electrochemical performance. Further compared the electrochemical performance with those of other graphene/carbon nanocomposites (GCNs) as well as carbon materials derived from natural materials, we found out that the well combination of graphene with biomolecules derived carbon is a critical factor to achieve good electrochemical performances. Therefore, our work provides a promising way to prepare well-combined GCN-S material for manufacturing the supercapacitors with both high performance and relative low-cost.

Experimental Section

Materials

Graphite powder (40μm) was obtained from Qingdao Henglide Graphite Co., Ltd. Concentrated H_2SO_4 (98%), $KMnO_4$, hydrazine hydrate, KOH, BSA, casein, gelatin were purchased from Sinopharm Chemical Reagent Co., Ltd. and used as received. The SF aqueous solution was prepared from *B. mori* silkworm cocoons followed a well-established procedure.[43] The final concentration of the SF aqueous solution was 4 wt%.

Preparation of GCN-S

The approach to generate GCN-S is illustrated in **Figure 1**. Firstly, $NH_3 \cdot H_2O$ was used to adjust the pH of GO and RSF aqueous solutions to 10, then GO solution was dripped into RSF solution with slowly stirring to get GO/SF mixture solution. The RGO/SF nanofibrils suspension was further obtained by a simple reduction reaction of hydrazine and GO/SF mixture solution. The resultant black suspension was quite even and stable up to 6 months without any precipitation at 4 °C (Figure S1 and S2). The RGO/SF nanofibrils suspension was then quenched by liquid N_2 and freeze-dried to gain the composite aerogel. Finally, the GCN-S was harvested through carbonization of the RGO/SF nanofibrils aerogels at 700 °C for 3 hours. To increase the specific surface area and create more pores in GCN-S, KOH was selected to activate our RGO/SF nanofibrils system under the same carbonization condition, and the final samples were named as GCN-S-X according to the weight ratio of KOH adding into complex suspension.[44] For example, GCN-S-0.5 means the weight ratio of KOH to complex suspension is 0.5. The detailed experimental procedure is shown in electronic supplementary information.

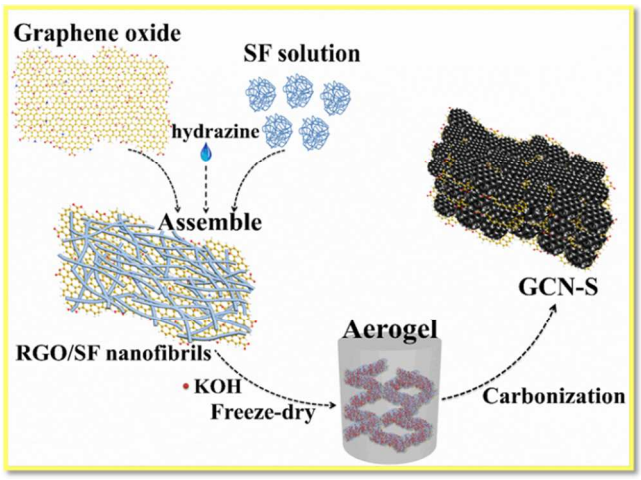

Figure 1. Illustration of the preparation of GCN-S

Electrochemical tests

All electrochemical characterizations were performed using a conventional three-electrode system equipped with an Hg/HgO reference electrode and a platinum counter electrode. The working electrode was prepared by mixing 80 wt% GCN material, 10 wt% carbon black, and 10 wt% PTFE to a viscous slurry, using the rod film machine to made it into a thin film and dried at 100 ^oC in an oven, then cut it into a small piece with 1cm×1cm and pressed onto a nickel foam current collector at 20 MPa. Cyclic voltammetry and galvanostatic charge/discharge measurements were performed within the potential range of -0.8 to 0 V vs. Hg/HgO on a CHI660E electrochemical workstation. The electrochemical impendance spectroscopy (EIS) was conducted using a Solartron Instrument Model 1287 electrochemical interface and 1255B frequency response analyzer controlled by a computer. The frequency limits were typically set between 0. 01 Hz to 100 KHz and the ac signal amplitude was 5 mV.

Characterizations

Transmission electron microscopy (TEM) experiments were conducted on a JEOL 2100F (Japan) or a Phillips CM20 (Netherlands) microscope both operated at 200 kV. Atomic force microscope (AFM) images were acquired using a Multimode 8 in the tapping mode. The morphology of samples was observed using a Hitachi S-4800 field-emission scanning electron microscope (FE-SEM). X-ray photoelectron spectroscopy (XPS) was acquired using a Kratos Axis Ultra DLD spectrometer (Kratos Analytical-A Shimadzu group company) equipped with a monochromatic Al Kα source (1486.6 eV). Thermal gravimetric analysis (TGA) was measured by a Pyris-1 thermal gravimetric analysis (TGA) with a heating rate of 20 ^oC min^{-1} under a nitrogen atmosphere from 50 to 700 ^oC. The specific surface areas (S_{BET}) were calculated by the Brunauer–Emmett–Teller (BET) method using the adsorption branch in a relative pressure range from 0.04 to 0.2. The micropore surface areas (S_m) were calculated using the V–t plot method. The total pore volumes (V_t) were the adsorbed amount at a P/P_0 of 0.992. The pore sizes (D_p) were derived from the adsorption branches of isotherms using the Barrett–Joyner–Halenda (BJH) model. X-ray powder diffraction (XRD) data were recorded on an X'pert Pro with Cu Kα radiation. Raman spectra were obtained with a Renishaw inVia Reflex spectrometer coupled to an Lieca microscope.

Results and Discussion

Characterization of RGO/SF nanofibrils suspension and GCN-S

Transmission electron microscopy (TEM) images show fully exfoliated RGO nanosheets in RGO/SF nanofibrils suspension with a rough surface (Figure 2a and S3). Atomic force microscopy (AFM) analysis further confirms that the RGO layers are fully covered by SF nanofibrils (Figure 2b, 2c). These evidences suggest that, although SF suffers slight degradation under our preparation procedure, it is still relatively stable and is able to assemble into nanofibrils. Interestingly, we observed two types of SF nanofibrils on RGO sheets in the same suspension. According to the AFM results, on those RGO sheets large than 10 μm, the tiny but dense SF nanofibrils with 100-300 nm in length and 1 nm in height are formed (Figure 2b and 2c). On the other hand, for smaller RGO sheets (lateral dimensions of several micrometers), the assembled SF nanofibrils with 1 μm in length and 2-3 nm in height twine RGO layers and more fibrils are surrounding like the flagellum of paramecium (Figure S4), which is consistent with our previous finding.[42] It is speculated that such distinction is closely related to the kinetic of SF nanofibrils formation on RGO, i.e. assembly mechanism and the relative concentration difference between RGO and SF. As we know, SF is constituted by chains containing alternating hydrophobic and hydrophilic blocks. Among them, the hydrophobic blocks consisted of highly conserved sequences of the repeat motif GAGAGS form anisotropic β-sheets.[45]

Thus RGO nanosheets with pure sp^2-hybridized carbon surfaces have strong hydrophobic interactions with the GAGAGS motifs, which is expected to promote SF assembled on RGO sheets. In other words, the hydrophobic surface of RGO can be considered as assembly sites for SF (the β-sheet formation sites). The larger RGO has enough hydrophobic area to provide more nucleation sites for the formation of β-sheet, so SF tends to assemble into shorter nanofibrils which is dominated by the β-sheet conformation. On the other side, the same amount of SF has to assemble into longer nanofibrils on the smaller RGO sheets as they lack the plenty space. Nevertheless, the formed SF nanofibrils in both cases sharply decrease the π-π stacking interaction of RGO sheets and then prevent the aggregation of RGO. Thus, RGO/SF nanofirbils can be well-dispersed in aqueous solution to be a stable suspension.

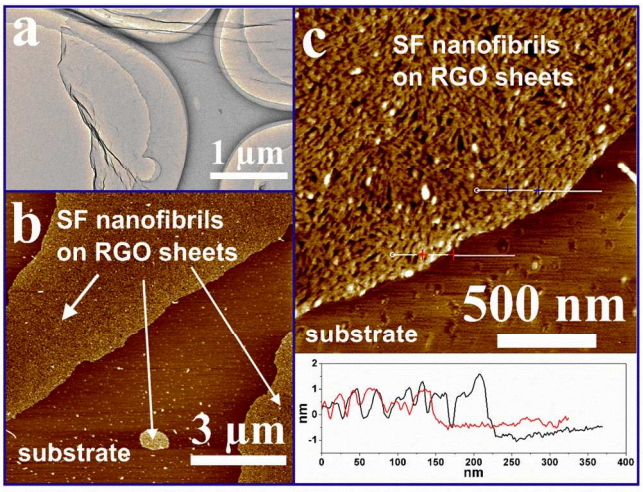

Figure 2. Structural characterization of RGO/SF nanofibrils suspensions. Transmission electron microscopy (TEM) images (a), AFM images and its height profile (b, c)

Figure 3a shows the morphology of RGO/SF nanofibrils composite aerogel after freeze-dried. The layered structure with no obviously distinguishing region between RGO and SF nanofibrils can be observed. As a comparison, we treated SF and GO in the same way but without reduce agent hydrazine, the resultant sample is heterogeneous, with large GO layers significantly separated by SF (balls and fibers) (Figure S5).

After carbonization of the aerogel, the layered structure still partly exists in GCN-S-0 (Figure 3b). The carbonized flakes show smooth surface with width of 1 μm. The control sample of C-SF (carbon derived from SF) was prepared by using pure SF solution through the same procedure. As shown in Figure S6, the carbonized flakes are about 10 μm wide that are much larger than those of GCN-S-0, and also display smooth surface. In the case of KOH involving, both GCN-S-0.5 and GCN-S-0.2, for example, present the similar morphologies to GCN-S-0 (Figure 3c, 3d and S7a-c) but much rougher surface. TEM images of these composites (Figure 3e, 3f and S7d-e) further confirm that the whole composite layer is uniformly covered by numerous meso/micropores.

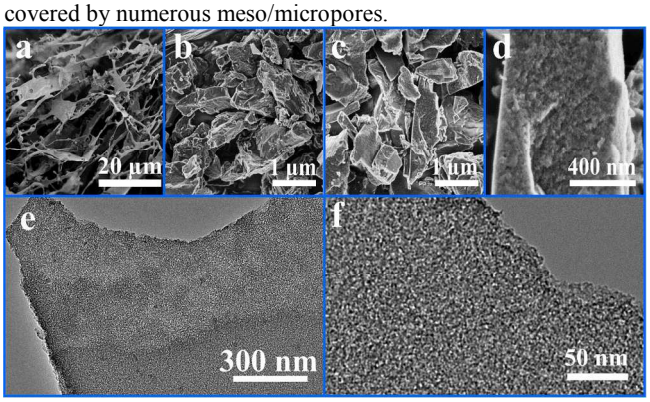

Figure 3. Scanning electron microscopy (SEM) images of the RGO/SF nanofibrils composite aerogel (a), GCN-S-0 (b), and GCN-S-0.5 and its magnifications (c, d). TEM images of GCN-S-0.5 at different viewing angles and magnifications (e, f).

Thermo gravimetric analysis (TGA) was employed to evaluate the proportion of graphene to SF derived carbon. As shown in Figure S8, the weight loss of SF and RGO is about 66% and 20% at 700 °C. Considering the original mass ratio of GO/SF is 1/50, the mass fraction of SF derived carbon and RGO is calculated to be 95.5% and 4.5% in the sample GCN-S-0, respectively. Then we further added a small amount of KOH solution into RGO/SF nanofibrils suspension for activation according to the reaction mechanism as follows: [44]

$$6KOH + 2C = 2K + 3H_2 + 2K_2CO_3 \quad (1)$$

$$K_2CO_3 = K_2O + CO_2 \quad (2)$$

$$CO_2 + C = 2CO \quad (3)$$

$$K_2CO_3 + 2C = 2K + 3CO \quad (4)$$

$$K_2O + C = 2K + CO \quad (5)$$

Figure 4a shows the nitrogen adsorption and desorption isotherm curves of GCN-S-0.5 and GCN-S-0.2. For GCN-S-0.5, the isotherm reveals similar type I isotherms to small H4 type hysteresis, which is the characteristic of microporous materials with mesopores.[44] The

Brunauer-Emmett-Teller (BET) specific surface area is 3.2×10^3 m^2g^{-1} [1] with the size of nanopores less than 5 nm (Figure 4b), and the majority pore sizes are located around 1.2 nm. Such distinctive morphology is significantly beneficial for the fast charge and mass transport at high current density without affecting the overall conductivity.[46] GCN-S-0.2 also presents typical type I isotherms, but with a smaller BET specific surface area of 1.6×10^3 m^2 g^{-1} due to the less nanopores. With increasing the amount of activation agent KOH, more mesopores are formed with the increase of the BET specific surface area. However, lots of previous works reported that there are no linear relationships among the activation agent content, the amount of micro/mesopore volume, and the specific surface area.[10, 16, 47] Moreover, the excessive activation agent would cause the structure breakage and reduce the overall surface area with a miserable yield. For example, when we mixed RGO/SF nanofibrils suspension (solid content = 1g) with different amount of KOH, the final product of GCN-S-0.2 is about 0.06 g and GCN-S-0.5 is 0.03 g. When we further increased the amount of KOH, we can hardly get any product. Therefore, this is commendable and meaningful that such an ultrahigh specific surface area is achieved with a very small amount of KOH addition in our work. The efficiency in such case is the best under the same amount of KOH addition as far as we know. We suppose that the high specific surface area probably attributes to the special composite aerogel structure as well as the homogeneous mixing in KOH activation procedure.

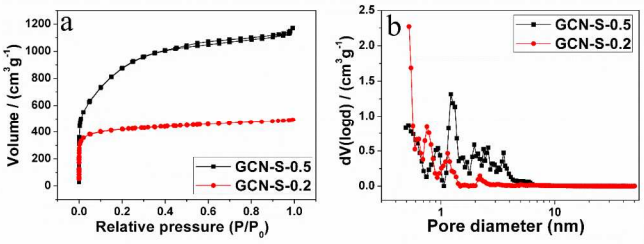

Figure 4. Nitrogen sorption isotherms (a) and pore size distribution curves (b) of GCN-S-0.5 and GCN-S-0.2, respectively.

As shown in Figure 5a, X-ray diffraction (XRD) and Raman spectroscopy were used to characterize the structural details of GCN-S. The power XRD patterns show a wide significant peak around 25° and a weak peak at around 43°, indicating the disordered carbon with low degree of crystallinity between graphite and amorphous carbon.[16] In addition, with the increasing amount of activation agent KOH, the peak around 25° shifts to lower 2 θ angle and its half width of peak becomes wider, indicating the increase of amorphous carbon with the destruction of graphite crystallization.[10] Furthermore, GCN-S-0.5 shows most strong low-angle scattering, which is in accord with the presence of a high density of micropores.[11] The Raman spectra in Figure 5b show the strong twin peaks around 1320 cm^{-1} and 1590 cm^{-1}. The peak around 1320 cm^{-1} is assigned to D band, which is due to the breathing mode of κ-point phonons of A_{1g} symmetry.[48] It comes from TO phonons around the Brillouin zone corner **K,** it is active by double resonance. Double resonance can also happen as an intravalley process, that is, connecting two points belonging to the same cone around **K**(or **K**´), that is the so-called D' peak.[49] The peak around 1590 cm^{-1} is assigned to G band, which includes G and D' peaks, G peak results from the E_{2g} phonon of sp^2 carbon atoms.[50] The single wide G band peak and D band with big FWHM (full-width at half-maximum) as well as the two small bumps between 2300 and 3200 cm^{-1} instead of well-defined second-order peaks (2D peak, D+D' peak, D+G peak) illustrate that our GCN-S material is more likely to be nanocrystalline graphite to low sp^3 amorphous carbon.[49] Furthermore, with the increase of KOH, the D/G intensity ratio of GCN-S-0, GCN-S-0.2, GCN-S-0.5 increases accordingly from 1.1, 1.17 to 1.21. Meanwhile, the FWHM of D and G band also becomes larger correspondingly. The results indicate that the more KOH we add, the more structure of GCN-S is likely to be low sp^3 amorphous carbon than nanocrystalline graphite, which is corresponded with the results from XRD.

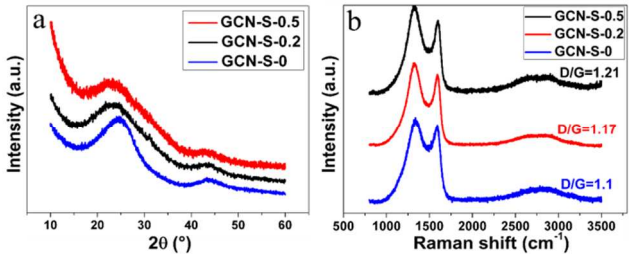

Figure 5. XRD patterns (a) and Raman spectra (b) of GCN-S-0, GCN-S-0.2 and GCN-S-0.5

Table 1 summarizes the chemical compositions of our GCN-S characterized by X-ray photoelectron spectroscopy (XPS), which are found to be consist of carbon, oxygen and nitrogen. N 1s spectra and O 1s spectra (Figure S9) show the chemical circumstance of these heteroatoms. Nitrogen atoms of our GCN-S can be divided into three types. The peaks at 398 eV, 400 eV and 401 eV are assigned to pyridinic (N-6), pyrrolic/pyridone (N-5) and quaternary (N-Q) nitrogen, respectively. The single peak around 531 eV in the O 1s spectra represents C=O quinone (O-I) type groups.[45] N-6, N-5 and O-I have been reported to have the most pronounced influence on the capacitance due to their pseudo-capacitive contributions, while N-Q shows enhanced effects on the capacitance due to its positive charge and thus causes an improved electron transfer, particularly at higher current loads.[51-53] With the large proportion of heteroatom doping, these samples could have better capacitance performance and wettability.

Table 1. Chemical composition of GCN-S determined by X-ray photoelectron spectroscopy (XPS)[a]

Sample	Nitrogen content (at %)				Oxygen content (at %)	Carbon content (at %)
	Total	N-6	N-5	N-Q		
GCN-S-0	5.27	1.17	2.41	1.69	9.34	85.38
GCN-S-0.2	5.05	1.10	1.53	2.41	6.96	87.99
GCN-S-0.5	2.95	0.29	1.52	1.14	12.39	84.66

[a] The data are the average of triplicate experiments.

The Electrochemical Performance of GCN-S

The electrochemical performance of the GCN-S for supercapacitors was analyzed in 6 mol/L KOH aqueous using a three-electrode system with an Hg/HgO reference electrode and a platinum counter electrode at room temperature. Figure 6a shows the comparison of the cyclic voltammetry (CV) curves of three types of GCN-S materials as well as the control sample C-SF at the same scan rate of 5 mV s^{-1} between -0.8 and 0 V (vs. Hg/HgO). Both GCN-S-0.5 and GCN-S-0.2 show a nearly rectangular shaped loop at all scan rates, confirming traditional double-layer capacitance characteristics.[54] The

humps (between -0.6 to -0.8 V) of these carbon materials are attributed to the pseudo-capacitive effect of incorporated heteroatoms and thus cause an increase in capacitance. The specific capacitance of GCN-S-0.5 and GCN-S-0.2 are much higher than that of GCN-S-0 and C-SF. Figure 6b-e further present the CV curves of these carbon materials at different scan rates, varying from 5 to 200 mV s^{-1} between -0.8 and 0 V (vs. Hg/HgO). Different from those of GCN-S-0 (Figure 6d) and C-SF (Figure 6e), the shapes of CV curves of GCN-S-0.5 (Figure 6b) and GCN-S-0.2 (Figure 6c) remain rectangular and present nearly 90° change at the switching potential even at high scan rate. In addition, there is only a tiny decrease of capacitance with the increase in scan rate, suggesting a high rate capability and a low internal resistance.[55] The tempting capacitor performance of GCN-S-0.5 and GCN-S-0.2 are mainly due to high SSA, proper pore size distribution and perfect combination of RGO/SF-derived carbon, which further brings the superb electro-conductivity.

The typical charge/discharge curves of GCN-S-0.5 and GCN-S-0.2 at a current rate in a range of 5 to 50 A g^{-1} are presented in Figure 7a and 7b. The charge/discharge curves demonstrate the typical triangle shape and almost no pronounced ohmic loss (IR drop) is observed. Figure 7c shows the rate capability performance of GCN-S evaluated by galvanostatic charge/discharge at different current rates, varying from 0.5 to 100 A g^{-1}. It can be found that both GCN-S-0.5 and GCN-S-0.2 have the great rate performance. For example, the capacitance of GCN-S-0.5 is 256 F g^{-1} at the current density of 0.5 A g^{-1} and still keeps 188 F g^{-1} at the current density of 50 A g^{-1}, with the retention rate of 73.4% compared with 0.5 A g^{-1}. It still delivers 163 F g^{-1} even at the current density of 100 A g^{-1}. However, it should be noticed that the increase in capacitance just with large SSA is relatively limited, because not all micropores are electrochemically accessible to form the electrical double-layer when they are immersed in electrolytes.[47] Therefore, the capacitance of GCN-S-0.5 is only a little higher than GCN-S-0.2, although it has much higher SSA. Furthermore, the long-term cyclic stability performance of GCN-S-0.5 and GCN-S-0.2 was tested at a current density of 5 A g^{-1} within a potential window of -0.8 to 0 V vs. Hg/HgO electrode in 6 mol L^{-1} KOH electrolyte. The results indicate that no evident capacitance loss occurs after 10000 charge–discharge cycles (Figure 7d). The capacitance retention ratio of GCN-S-0.5 and GCN-S-0.2 is 96.3% and 97.9% respectively, which strongly demonstrates the excellent electrochemical stability of such graphene-carbon nanocomposite materials.

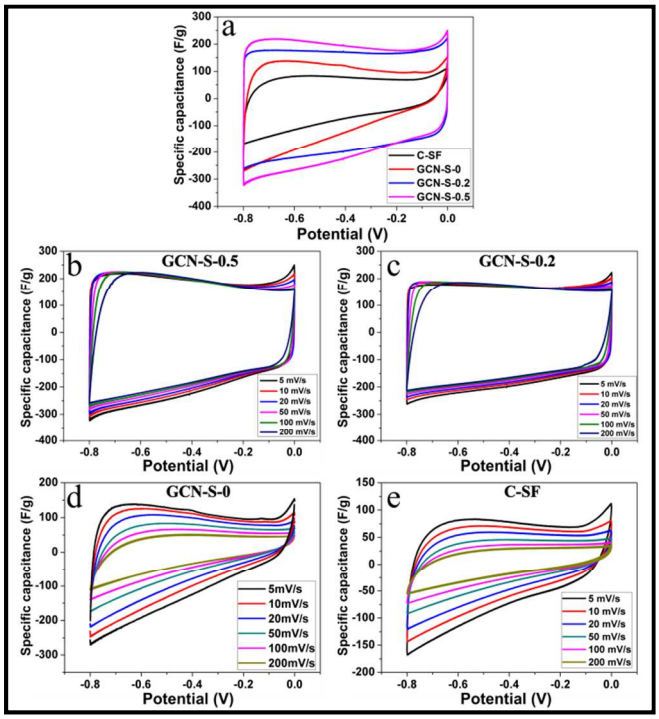

Figure 6. CV comparison of these carbon materials at the scan rate of 5 mV s^{-1} (a); The CV curves of GCN-S-0.5 (b), GCN-S-0.2 (c), GCN-S-0 (d) and C-SF (e) at different scan rates varying from 5 mV s^{-1} to 200 mV s^{-1} in 6 mol/L KOH aqueous solution.

The electrochemical impedance spectroscopy (EIS) measurement also proves the excellence of capacitive profile (Figure 7e and 7f) of GCN-S-0.5 and GCN-S-0.2. Both GCN-S-0.5 and GCN-S-0.2 reveal the very similar Nyquist plots composed of two regions, including a semicircle at high frequency and a nearly vertical line along the imaginary axis at low frequency. The semicircle is related to the diffusion layer, which is governed by the ability of ion migration through the pores and electrical resistivity of the electrode material.[56] This diffusion layer consists of a parallel combination of constant phase element (CPE) and a series of interface resistance (R_i) and Warburg resistance (W). R_i is interface resistance created on the diffusion layer, which significantly affects the IR drop and rate capability, while W represents the hindrance in electrolyte diffusion through porous network of the electrode.[57,58] Both Figure 7d and 6e show ultrasmall semicircle radius at high frequency, which prove good conducting behaviors of our materials. The nearly vertical lines along the imaginary axis further point out the terrific capacitive behavior. EIS results correspond well with the excellent rate capability, and the equivalent series resistance (ESR) of GCN-S-0.5 and GCN-S-0.2 is calculated to around 0.55 Ω and 0.84 Ω, respectively. All of these events clearly demonstrate that our GCN-S materials have excellent properties for supercapacitors. These brilliant performances are mainly because of the large specific surface areas and proper pore size distribution of GCN-S, as well as the perfect combination of SF-derived carbon and RGO. Both of the advantages can be traced to the well-assembled RGO/SF nanofibrils layered structures, which ensures the excellent electroconductibility of final GCN-S.

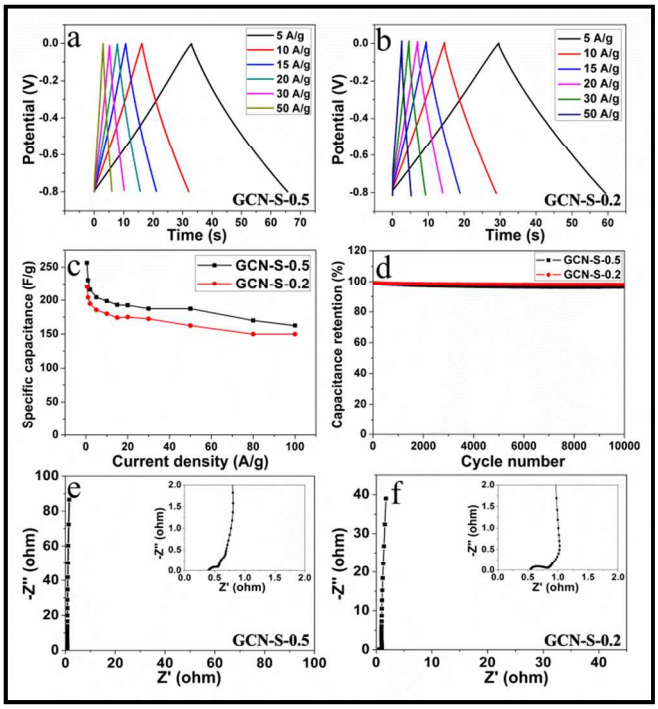

Figure 7. Galvanostatic charge–discharge curves of GCN-S-0.5 (a) and GCN-S-0.2 (b) at the current density from 5 to 50 A g^{-1}; Rate performance of GCN-S-0.5 and GCN-S-0.2 at different current densities varying from 0.5 to 100 A g^{-1} (c); The cycle performance of GCN-S-0.5 and GCN-S-0.2 at the current density of 5 A g^{-1}(d); Electrochemical impedance spectra (inset: magnified 0–2 Ω region) of GCN-S-0.5 (e) and GCN-S-0.2 (f).

Moreover, the energy and power densities for our GCN-S based supercapacitors are depicted in the Ragone plot (Figure 8). Both GCN-S-0.5 and GCN-S-0.2 could achieve high energy density. For example, the maximum energy density of GCN-S-0.5 can be achieved as 22.8 Wh kg^{-1} at a power density of 200 W kg^{-1}. Usually the increase of power density compromises the energy density value, but in our case, there is only a slight decrease in the energy density. Even at high power density of 40000 W kg^{-1}, the energy density of GCN-S-0.5 still reaches 14.4 Wh kg^{-1}. Such results are much better than the energy density of most commercially available supercapacitors (less than 10 Wh kg^{-1}, mostly only 3-4 Wh kg^{-1}),[1,43] and higher than many previously reported carbon based devices, such as other activated carbon derived from biomass,[59-60] activated RGO,[61] nitrogen-doped porous carbon nanofibers,[62] and sponge-like graphene.[63]

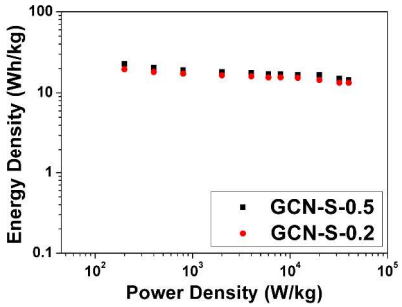

Figure 8. Ragone plot of GCN-S-0.5 and GCN-S-0.2 based supercapacitors.

In order to further investigate the importance between well-combination of RGO with protein based carbon sources as well as the electrochemical performance of the corresponded carbon materials, we tried other fibrous protein (gelation) and globulins (BSA and casein). It is found that all these proteins could stabilize RGO during reduction process and prevent it from heavily precipitation to a certain extent. However, the final suspension involved these proteins are not as stable as SF. As for RGO/globulin (either BSA or casein) system, the distinct precipitation could be observed at the bottom of the suspension after a few hours. As for RGO/gelation system, the composite suspension turns into three layers after a few hours (Figure S11). The top layer and the middle layer form into almost transparent gel and non-transparent black gel, respectively, while the bottom layer is a dark precipitate. Further AFM investigations show that there is no composite structure formed between BSA and RGO while BSA only surrounds RGO (Figure S10), and gelatin randomly attaches on both RGO layers and mica matrix (Figure S12a, S12b) rather than selectively and fully covering on RGO to produce the nanocomposite like SF nanofibrils do, which lead to the limited stabilizing ability.

We further prepared GCN-G-0.2 (graphene/gelation based carbon nanocomposites) under the same condition of GCN-S-0.2 to investigate its electrochemical performance (Figure S12c and S12d). The results show that, although GCN-G-0.2 has higher capacitance than GCN-S-0.2 at a relatively lower current density (0.2 A g^{-1}), at high current density, the capacitance of GCN-G-0.2 is much lower. It illustrates that the lower capacitance at high current density of GCN-G-0.2 is not caused by the smaller pseudo-capacitance and the most reasonable explanation is the poor combination between RGO and gelatin fibers which leads to a large part of capacitance not pronounced, which strongly confirms our hypothesis. Obviously, this result signifies the importance of well-combination of RGO with carbon source.

For comparison, we also prepared heteroatom-doped carbon materials from freeze-dried regenerate silk fibroin and degummed silk in the similar activation procedure with most of the literature reported. Briefly, these materials were pre-carbonized at 350 °C for 2 hours, then mixed with KOH (weight $_{KOH}$: weight $_{carbon}$ = 1 : 1) and further carbonized at 800 °C for 2 hours. The final products were named as CMs-FD-SF (carbon materials from freeze-dried regenerate silk fibroin) and CMs-D-Silk (carbon materials from degummed silk).

We compared electrochemical performances of various GCNs in our case with other GCNs as well as carbon materials derived from natural materials (Table 2). It can be seen that the capacitance of those heteroatom-doped carbon materials in the literatures as well as CMs-D-Silk show high values at the small current density due to the redox process of electroactive materials, but decreases sharply with the increase of current density. Interestingly, GCN-S maintains high capacitance with increasing current density, e.g. keeps 188 F g^{-1} at the current rate of 50 A g^{-1}, and its rate capability is much better than those of the others. The similar results can be derived from the comparison of the CV curves (Figure 6a, Figure 6b and Figure S13). It illustrates that the well-combination of graphene with SF nanofibrils, which turned out to be micro/meso carbon after activation, is a very crucial factor to ensure good electrochemical performance of the final material. The extraordinary rate performance, high capacitance especially at the high current density and the ultra-small impedance make our GCN-S the prefect material for supercapacitors.

Table 2. Comparison of the properties of carbon materials derived from natural materials and their use in supercapacitors

Materials	Activating agent / mass ratio with the pre-carbon material	Activated temperature/ carbonization temperature	Capacitance at 1 A g^{-1} / F g^{-1}	Capacitance at 10 A g^{-1} /F g^{-1}	Capacitance at 50 A g^{-1} /F g^{-1}	Capacitance of 100 A g^{-1} /F g^{-1}	Electrolyte
GCN-S-0.5	KOH/0.5	700	230	199	188	163	6M KOH
GCN-S-0.2	KOH/0.2	700	204	180	163	150	6M KOH
GCN-G-0.2	KOH/0.2	700	163	135	119	100	6M KOH
CMs-D-Silk[a]	KOH/1	800	230	190	144	110	6M KOH
CMs-FD-SF[b]	KOH/1	800	152	123	63	NG	6M KOH
H-CMNs from RSF[10]	KOH/1	700	About 220	About 155	120	NG	1 M H_2SO_4
Human hair-derived carbon[11]	KOH/2	700	About 310	196	Less than 100	NG	6M KOH
		800	About 340	227	About 160	NG	
Carbon from cellulose[14]	KOH/4	700	About 170	About 125	NG	NG	1M $TEABF_4$ solution in AN
		800	About 120	About 105	NG	NG	
Carbon from wood sawdust[14]	KOH/4	700	About 170	About 150	NG	NG	1M $TEABF_4$ solution in AN
		800	About 190	About 180	NG	NG	
Carbon from potato starch[14]	KOH/4	700	About 160	About 130	NG	NG	1M $TEABF_4$ solution in AN
Carbon from pollens lotus[15]	KOH/4	900	207	About 190	NG	NG	$EMIMBF_4$
Carbon from cow dung[16]	KOH/2	800	117	NG	NG	NG	1.0 M Et_4NBF_4 in AN
Carbon from GO and lignin[64]	KOH/4	800	213	183	NG	NG	$EMIMBF_4$

[a,b](The detailed electrochemical performance is shown in electronic supplementary information Figure S13 and S14.)

Conclusions

In this study, we developed a novel GCN-S material with high specific surface area, multi-porous structure and fairly good electrical conductivity through the carbonization of the RGO and SF nanocomposite involved KOH. By taking full use of the SF assembly on RGO sheets, only a small amount of KOH was employed for activation, which highly improved the ultimate yield. The well combination of RGO and SF nanofibrils also endow the obtained GCN-S materials with excellent electrochemical performance. It is displayed that the specific capacitance of GCN-S-0.5 was 256 F g^{-1} at the current density of 0.5 A g^{-1} and significantly kept 188 F g^{-1} with the retention rate up to 73.4% after a 100-fold increasing at current density of 50 A g^{-1}. Meanwhile, the ESR of GCN-S-0.5 and GCN-S-0.2 was as low as 0.55 Ω and 0.84 Ω, respectively. After charge–discharge rate of 5 A g^{-1} for 10000 cycles, the GCN-S-0.5 and GCN-S-0.2 still exhibit remarkable electrochemical stability with the capacitance retention ratio of 96.3% and 97.9%, respectively. Furthermore, the GCN-S-0.5 based supercapacitor could achieve high energy density up to 14.4 Wh kg^{-1} even at super high power density of 40000 W kg^{-1}. The work presented here provides an efficient way to prepare the promising material for high performance and relative low-cost supercapacitors.

Acknowledgements

This work was supported by National Natural Science Foundation of China (NSFC 21034003) and Program of Shanghai Subject Chief Scientist (12XD1401000). We thank Dr. Chao Gao and Li Peng at Zhejiang University for their generously providing GO. We also thank Dr. Jinrong Yao, Dr. Jianchuan Wen and Dr. Shengjie Ling for their valuable suggestions and discussions of our work.

Notes and references

[a] Yaxian Wang, Yu Wang, Prof. Dr. Xin Chen, Prof. Dr. Zhengzhong Shao
Department of Macromolecular Science
Fudan University
Shanghai 200433, China
E-mail: zzshao@fudan.edu.cn
[b] Yanfang Song，Prof. Dr.Yongyao Xia
Department of Chemistry and Shanghai Key Laboratory of Molecular Catalysis and Innovative Materials
Institute of New Energy,Fudan University
Shanghai 200433, China

Electronic Supplementary Information (ESI) available: The detailed experimental procedure; Photograph of GO/SF, RGO/SF and RGO in different conditions; Characterizations of RGO/SF nanofibrils (Raman spectra, TEM, AFM, SEM images); SEM image of C-SF; SEM and TEM images GCNs-0.2; TGA curves of silk, RGO and RGO/SF nanofibrils composite aerogel; XPS spectra for N1s and O1s of GCNs; AFM images of RGO and BSA; Photograph of RGO/gelatine, RGO/casein and RGO/BSA; AFM images of RGO/gelatin; DC curves and rate performance of GCN-G-0.2; The CV curves of CMs-FD-SF and CMs-D-Silk; Rate performance of CMs-FD-SF and CMs-D-Silk].

1 G. P. Wang, L. Zhang and J. J. Zhang, *Chem. Soc. Rev.*, 2012, **41**, 797.

2 S. L. Candelaria, Y. Y. Shao, W. Zhou, X. Li, J. Xiao, J. Zhang, Y. Wang, J. Liu, J. H. Li and G. Z. Cao, *Nano Energy*, 2012, **1**, 195.
3 Y. P. Zhai, Y. Q. Dou, D. Y. Zhao, P. F. Fulvio, R. T. Mayes and S. Dai, *Adv. Mater.*, 2011, **23**, 4828.
4 Y. Huang, J. J. Liang and Y. S. Chen, *Small*, 2012, **8**, 1805.
5 P. Simon and Y. Gogotsi, *Nat. mater.*, 2008, **7**, 845.
6 L. L. Zhang, R. Zhou and X. S. Zhao, *J. Mater. Chem.*, 2010, **20**, 5983.
7 A. Davies and A. Yu, *The Canadian Journal of Chemical Engineering*, 2011, **89**, 1342.
8 G. H. Yu, X. Xie, L. J. Pan, Z. N. Bao and Y. Cui, *Nano Energy*, 2013, **2**, 213.
9 B. Zheng, T. W. Chen, F. N. Xiao, W. J. Bao and X. H. Xia, *J. Solid State Electr.*, 2013, **17**, 1809.
10 Y. S. Yun, S. Y. Cho, J. Shim, B. H. Kim, S. Chang, S. J. Baek, Y. S. Huh, Y. Tak, Y. W. Park, S. Park and H. Jin, *Adv. Mater.*, 2013, **25**, 1993.
11 W. J. Qian, F. X. Sun, Y. H. Xu, L. H. Qiu, C. H. Liu, S. D. Wang and F. Yan, *Energy Environ. Sci.*, 2013, **7**, 379.
12 Z. Li, Z. W. Xu, X. H. Tan, H. L. Wang, C. M. B. Holt, T. Stephenson, B. C. Olsen and D. Mitlin, *Energy Environ. Sci.*, 2013, **6**, 871.
13 M. Biswal, A. Banerjee, M. Deo and S. Ogale, *Energy Environ. Sci.*, 2013, **6**, 1249.
14 L. Wei, M. Sevilla, A. B. Fuertes, R. Mokaya and G. Yushin, *Adv. Energy Mater.*, 2011, **1**, 356.
15 L. Zhang, F. Zhang, X. Yang, K. Leng, Y. Huang and Y. S. Chen, *Small*, 2013, **9**, 1342.
16 D. Bhattacharjya and J. S. Yu, *J. Power Sources*, 2014, **262**, 224.
17 H. Jiang, P. S. Lee and C. Z. Li, *Energy Environ. Sci.*, 2012, **6**, 41.
18 H. Choi, S. Jung, J. Seo, D. W. Chang, L. Dai and J. Baek, *Nano Energy*, 2012, **1**, 534.
19 X. M. Sun, H. Sun, H. P. Li and H. S. Peng, *Adv. Mater.*, 2013, **25**, 5153.
20 J. X. Zhu, D. Yang, Z. Y. Yin, Q. Y. Yan and H. Zhang, *Small*, 2014, **10**, 3480.
21 J. Chen, C. Li and G. Q. Shi, *J. Phys. Chem. Lett.*, 2013, **4**, 1244.
22 T. Kuilla, S. Bhadra, D. Yao, N. H. Kim, S. Bose and J. H. Lee, *Prog. Polym. Sci.*, 2010, **35**, 1350.
23 Y. Wang, Z. Q. Shi, Y. Huang, Y. F. Ma, C. Y. Wang, M. M. Chen and Y. S. Chen, *J. Phys. Chem. C*, 2009, **113**, 13103.
24 X. J. Wan, Y. Huang and Y. S. Chen, *Accounts Chem. Res.*, 2012, **45**, 598.
25 J. Yan, Z. J. Fan, T. Wei, W. Z. Qian, M. L. Zhang and F. Wei, *Carbon*, 2010, **48**, 3825.
26 Z. Y. Zhang, F. Xiao, L. H. Qian, J. W. Xiao, S. Wang and Y. Q. Liu, *Adv. Energy Mater.*, DOI: 10.1002/aenm.201400064.
27 W. Lv, F. Sun, D. M. Tang, H. T. Fang, C. Liu, Q. H. Yang and H. M. Cheng, *J. Mater. Chem.*, 2011, **21**, 9014.
28 H. H. Chang, C. K. Chang, Y. C. Tsai and C. S. Liao, *Carbon*, 2012, **50**, 2331.
29 H. P. Cong, X. C. Ren, P. Wang and S. H. Yu, *Energy Environ. Sci.*, 2013, **6**, 1185.
30 Q. Wu, Y. X. Xu, Z. Y. Yao, A. R. Liu and G. Q. Shi, *ACS Nano*, 2010, **4**, 1963.
31 L. H. Tang, H. X. Chang, Y. Liu and J. H. Li, *Adv. Funct. Mater.*, 2012, **22**, 3083.
32 T. H. Han, W. J. Lee, D. H. Lee, J. E. Kim, E. Choi and S. O. Kim, *Adv. Mater.*, 2010, **22**, 2060.
33 J. B. Liu, S. H. Fu, B. Yuan, Y. L. Li and Z. X. Deng, *J. Am. Chem. Soc.*, 2010, **132**, 7279.
34 H. X. Chang and H. K. Wu, *Energy Environ. Sci.*, 2013, **6**, 3483.
35 D. Khatayevich, T. Page, C. Gresswell, Y. Hayamizu, W. Grady and M. Sarikaya, *Small*, 2014, **10**, 1505.
36 S. Myung, P. T. Yin, C. Kim, J. Park, A. Solanki, P. I. Reyes, Y. Lu, K. S. Kim and K. Lee, *Adv. Mater.*, 2012, **24**, 6081.
37 C. X. Li, J. Adamcik and R. Mezzenga, *Nat. Nanotechnol.*, 2012, **7**, 421.
38 A. Erdem, E. Eksin and M. Muti, *Colloid Surf. B-Biointerfaces*, 2014, **115**, 205.
39 D. Blond, D. N. McCarthy, W. J. Blau and J. N. Coleman, *Biomacromolecules*, 2007, **8**, 3973.
40 K. Hu, M. K. Gupta, D. D. Kulkarni and V. V. Tsukruk, *Adv. Mater.*, 2013, **25**, 2301.
41 L. Huang, C. Li, W. J. Yuan and G. Q. Shi, *Nanoscale*, 2013, **5**, 3780.
42 S. J. Ling, C. X. Li, J. Adamcik, S. H. Wang, Z. Z. Shao, X. Chen and R. Mezzenga, *ACS Macro Lett.*, 2014, **3**, 146.
43 G. Q. Zhou, Z. Z. Shao, D. P. Knight, J. P. Yan and X. Chen, *Adv. Mater.*, 2009, **21**, 366.
44 Y. W. Zhu, S. Murali, M. D. Stoller, K. J. Ganesh, W. W. Cai, P. J. Ferreira, A. Pirkle, R. M. Wallace, K. A. Cychosz, M. Thommes, D. Su, E. A. Stach and R. S. Ruoff, *Science*, 2011, **332**, 1537.
45 H. Guo, J. M. Zhang, T. Xu, Z. D. Zhang, J. R. Yao and Z. Z. Shao, *Biomacromolecules*, 2013, **14**, 2733.
46 V. Ruiz and A. G. Pandolfo, *J. Power Sources*, 2011, **196**, 7816.
47 J. Yan, Q. Wang, T. Wei and Z. Fan, *Adv. Energy Mater.*, DOI: 10.1002/aenm.201300816
48 A. C. Ferrari and J. Robertson, *Phys. Rev. B*, 2000, **61**, 14095.
49 A. C. Ferrari and D. M. Basko, *Nat. Nanotechnol.*, 2013, **8**, 235.
50 C. N. R. Rao, A. K. Sood, K. S. Subrahmanyam and A. Govindaraj, *Angew. Chem. Int. Ed.*, 2009, **48**, 7752.
51 D. Hulicova-Jurcakova, M. Seredych, G. Q. Lu and T. J. Bandosz, *Adv. Funct. Mater.*, 2009, **19**, 438.
52 Y. Tan, C. F. Xu, G. X. Chen, Z. H. Liu, M. Ma, Q. J. Xie, N. F. Zheng and S. Z. Yao, *ACS Appl. Mater. Interfaces*, 2013, **5**, 2241.
53 M. Seredych, D. Hulicova-Jurcakova, G. Q. Lu and T. J. Bandosz, *Carbon*, 2008, **46**, 1475.
54 Z. H. Wen, X. C. Wang, S. Mao, Z. Bo, H. Kim, S. Cui, G. H. Lu, X. L. Feng and J. H. Chen, *Adv. Mater.*, 2012, **24**, 5610.
55 Y. F. Song, D. D. Zhou, Y. G. Wang, C. X. Wang and Y. Y. Xia, *New J. Chem.*, 2013, **37**, 1768.
56 Q. Cheng, J. Tang, J. Ma, H. Zhang, N. Shinya and L. C. Qin, *Carbon*, 2011, **49**, 2917.
57 L. L. Zhang and X. S. Zhao, *Chem. Soc. Rev.*, 2009, **38**, 2520.
58 P. L. Taberna, P. Simon and J. F. Fauvarque, *J. Electrochem. Soc.*, 2003, **150**, A292.
59 T. E. Rufford, D. Hulicova-Jurcakova, K. Khosla, Z. Zhu and G. Q. Lu, *J. Power Sources*, 2010, **195**, 912.
60 T. E. Rufford, D. Hulicova-Jurcakova, Z. Zhu and G. Q. Lu, *Electrochem. Commun.*, 2008, **10**, 1594.
61 L. L. Zhang, X. Zhao, M. D. Stoller, Y. W. Zhu, H. X. Ji, S. Murali, Y. P. Wu, S. Perales, B. Clevenger and R. S. Ruoff, *Nano Lett.*, 2012, **12**, 1806.
62 L. F. Chen, X. D. Zhang, H. W. Liang, M. G. Kong, Q. F. Guan, P. Chen, Z. Y. Wu and S. H. Yu, *ACS Nano*, 2012, **6**, 7092.
63 Z. W. Xu, Z. Li, C. M. B. Holt, X. H. Tan, H. L. Wang, B. S. Amirkhiz, T. Stephenson and D. Mitlin, *J. Phys. Chem. Lett.*, 2012, **3**, 2928.
64 F. Zhang, Y. H. Lu, X. Yang, L. Zhang, T. F. Zhang, K. Leng, Y. P. Wu, Y. Huang, Y. F. Ma and Y. S. Chen, *Small*, 2014, **10**.

Table of contents entry

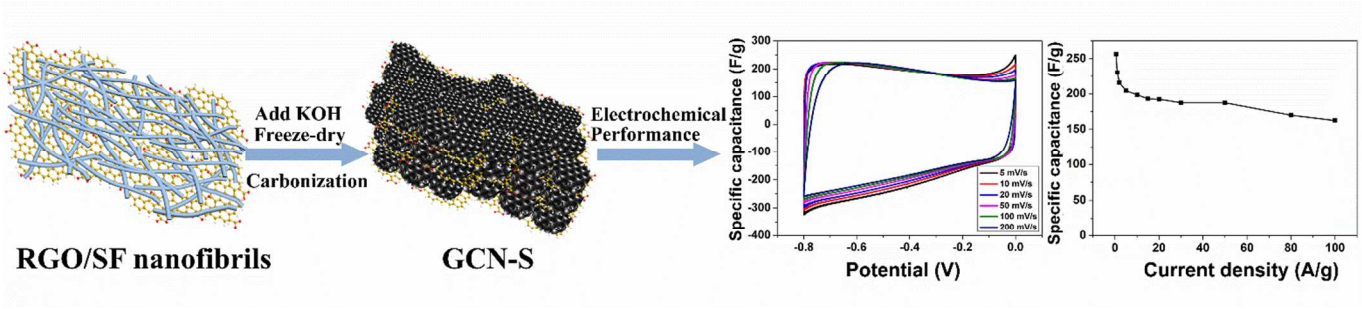

A novel way is provided to harvest a high performance graphene/silk fibroin based carbon (GCN-S) material for supercapacitors.